Astronomy & Astrophysics manuscript no. 3910 February 5, 2008
(DOI: will be inserted by hand later)

Kinematics and star formation activity in the $z_{\rm abs}$ = 2.03954 damped Lyman-α system towards PKS 0458−020⋆

Janine Heinmüller[1,2,3], Patrick Petitjean[1,4], Cédric Ledoux[5], Sara Caucci[1], and R. Srianand[6]

[1] Institut d'Astrophysique de Paris, UMR7095 CNRS, Université Pierre & Marie Curie, 98bis Boulevard Arago, 75014, Paris, France
[2] Astronomisches Rechen-Institut, Zentrum für Astronomie der Universität Heidelberg, Mönchhofstr. 12-14, 69120 Heidelberg, Germany
[3] Astrophysik, Universität Potsdam, Am Neuen Palais 10, 14469 Potsdam, Germany
[4] LERMA, Observatoire de Paris, 61 Avenue de l'Observatoire, 75014, Paris, France
[5] European Southern Observatory, Alonso de Córdova 3107, Casilla 19001, Vitacura, Santiago, Chile
[6] IUCAA, Post Bag 4, Ganesh Khind, Pune 411 007, India

Received 25 July 2005; accepted 16 November 2005

Abstract. We present UVES observations of the log N(H I) = 21.7 damped Lyman-α system at $z_{\rm abs}$ = 2.03954 towards the quasar PKS 0458−020. H I Lyman-α emission is detected in the center of the damped Lyman-α absorption trough. Metallicities are derived for Mg II, Si II, P II, Cr II, Mn II, Fe II and Zn II and are found to be −1.21 ± 0.12, −1.28 ± 0.20, −1.54 ± 0.11, −1.66 ± 0.10, −2.05 ± 0.11, −1.87 ± 0.11, −1.22 ± 0.10, respectively, relative to solar. The depletion factor is therefore of the order of [Zn/Fe] = 0.65. We observe metal absorption lines to be blueshifted compared to the Lyman-α emission up to a maximum of ∼100 and 200 km s^{-1} for low and high-ionization species respectively. This can be interpreted either as the consequence of rotation in a large (∼7 kpc) disk or as the imprint of a galactic wind. The star formation rate (SFR) derived from the Lyman-α emission, 1.6 M$_\odot$yr^{-1}, is compared with that estimated from the observed C II* absorption. No molecular hydrogen is detected in our data, yielding a molecular fraction log $f < -6.52$. This absence of H_2 can be explained as the consequence of a high ambient UV flux which is one order of magnitude larger than the radiation field in the ISM of our Galaxy and originates in the observed emitting region.

Key words. cosmology: observations – galaxies: ISM – quasars: absorption lines – quasars: individual: PKS 0458−020

1. Introduction

Damped Lyman-α (DLA) systems are characterized by neutral hydrogen column densities of N(H I) $\geq 2 \times 10^{20}$ atoms cm^{-2} determined from the damping wings of the H I Lyman-α absorption line. Due to the large H I column densities and the conspicuous presence of metals, DLAs are believed to arise in intervening galaxies. At low and intermediate redshifts, galaxy counterparts have been found in a number of cases (Le Brun et al. 1997; Chen & Lanzetta 2003). Although it is probable that at high redshift DLAs are associated with regions of star formation, it turns out to be difficult to detect them in emission. Despite intensive searches, very few cases have been found so far in which Lyman-α is seen in emission at the same redshift as the absorption (e.g., Møller & Warren 1993; Møller et al. 1998; Warren et al. 2001; Vreeswijk et al. 2004). One of these rare cases is the $z_{\rm abs}$ = 2.03954 DLA system towards PKS 0458−020 where Lyman-α emission from the corresponding absorbing galaxy has recently been detected by Møller et al. (2004) in the center of the absorption trough. This DLA system is well known as it was one of the first to be detected in absorption in 21 cm observations (Wolfe et al. 1985).

In this paper, we present a new high-resolution spectrum of this quasar that allows us to discuss the kinematics of the Lyman-α emission line relative to the metal lines belonging to the DLA system. We measure metallicities and depletion factors. We discuss and compare two independent methods for the derivation of the star formation rate, one based on the Lyman-α emission line and one using the C II* absorption line. Also, we focus on the physical conditions in the DLA and investigate the absence of molecular hydrogen.

2. Observations and data reduction

The Ultraviolet and Visible Echelle Spectrograph (UVES; Dekker et al. 2000), mounted at the Nasmyth B focus of the ESO Kueyen VLT-UT 2 8.2 m telescope on Cerro Paranal in

⋆ Based on observations carried out at the European Southern Observatory (ESO), under visitor mode progs. ID 66.A-0624, 68.A-0600 and 072.A-0346, with the UVES echelle spectrograph installed at the ESO Very Large Telescope (VLT), unit Kueyen, on mount Paranal (Chile).

Chile, was used during three visitor mode observing runs. Dichroic beam splitters were used on October 21-23, 2000, and October 16, 2001, to observe at the same time with both spectroscopic arms. During these two runs, central wavelengths were adjusted to 437 nm in the blue arm and 570, 580 or 750 nm in the red arm. Full wavelength coverage was obtained this way between 376 and 939 nm with only a small gap between 741 and 757 nm due to the physical gap between the two red arm CCDs. The CCD pixels were binned 2×2 and the slit widths were fixed to $1''$, yielding, under the $0\farcs6$ seeing conditions achieved during the observations, a resolving power $R \approx 53,000$. The total integration time on source was about 3.5 h. Complementary observations at wavelengths shorter than 387 nm down to the atmospheric cutoff ($\sim$ 305 nm) were obtained on October 29-30, 2003, using the blue arm of UVES in standalone together with the standard setting with central wavelength adjusted to 346 nm. During this third run, due to the faintness of the QSO the CCD pixels were binned 2×3, while the slit width again was fixed to $1''$. These additional observations amount to a total of about 3.5 h split in three different exposures.

The data were reduced using the latest version of the UVES pipeline (Ballester et al. 2000) which is available as a dedicated component of the ESO MIDAS data reduction system. The main characteristics of the pipeline are to perform a precise inter-order background subtraction for science frames and master flat-fields, and an optimal extraction with Gaussian modeling of the object spatial profile rejecting cosmic ray impacts and subtracting the sky spectrum simultaneously. The pipeline products were checked step by step. The wavelength scale of the spectra reduced by the pipeline was then converted to vacuum-heliocentric values and individual 1-D spectra were scaled, weighted and combined to produce the final science spectrum and its associated variance.

3. The Lyman-α emission

By fitting the damped wings, we measure the column density of the damped Lyman-α absorption to be log N(H I) = 21.7±0.1. H I Lyman-α in emission is detected in the center of the broad absorption as can be seen in Fig. 1. Since the emission line profile is affected by noise we applied different smoothing factors to the spectrum to measure the exact wavelength of the Lyman-α emission. In Fig. 2, the initial spectrum of the Lyman-α emission line is shown together with the results of applying smoothing with different smoothing radii. As can be seen the position of the peak of the line slightly depends on the smoothing radius. The line is not symmetric, probably because of absorption by intervening neutral hydrogen in the blue wing. We therefore choose the peak of the line as an indicator of the mean position of the emission, 3695.6±0.2 Å (errors are estimated from the shifts due to different smoothing). This corresponds to an emission redshift of $z = 2.0400 \pm 0.0002$.

Our spectrum is not flux calibrated. We checked that the flux in the Lyman-α emission line relative to the continuum from the quasar is about the same as in the spectrum of Møller et al. (2004). The measured Lyman-α flux from Møller et al. (2004) is $F = 5.4^{+2}_{-0.8} \times 10^{-17}$ erg s^{-1} cm^{-2}. Assuming $H_0 = 70$ km s^{-1} Mpc^{-1}, $\Omega_M = 0.3$ and $\Omega_\Lambda = 0.7$, the redshift $z = 2.0400$ corresponds to a luminosity distance of $d_L = 15921$ Mpc. The observed flux therefore corresponds to a Lyman-α luminosity of $L_{Ly\alpha} = 1.64 \times 10^{42}$ erg s^{-1}. Adopting the relation between the measured Lyman-α luminosity and the star formation rate from Kennicutt et al. (1998), $L_{Ly\alpha} = 10^{42} \times$ SFR , we derive a star formation rate of SFR = $1.6^{+0.6}_{-0.3}$ M$_\odot$ yr^{-1}. The Lyman-α emission provides only a lower limit to the SFR as the presence of dust can reduce the strength of the Lyman-α emission. In the following section, we will see that the depletion factor is not small and that dust is present in the gas.

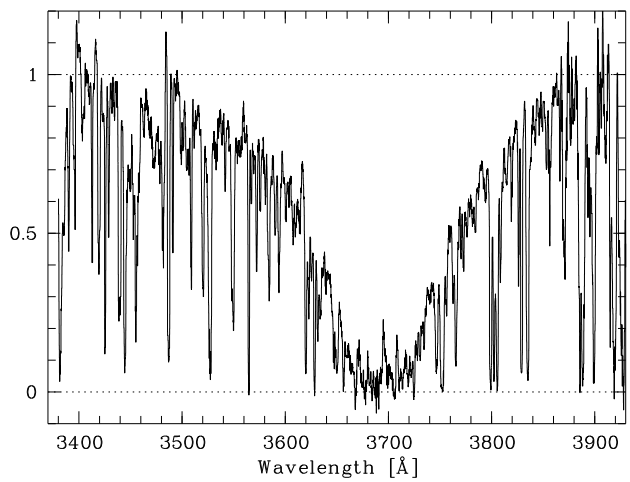

Fig. 1. UVES spectrum of PKS 0458−020 in the wavelength interval between 3400 and 3900 Å showing the damped Lyman-α line with the Lyman-α emission line in the center. The original spectrum was smoothed with a Gaussian filter of FWHM 10 pixels. The neutral hydrogen column density of the system, obtained by Voigt profile fitting of the absorption trough, is log N(H I) = 21.7. An emission line is detected in the center of the absorption trough.

4. Column densities and metallicities

A number of metal absorption lines associated with the DLA system are detected: low-ionization species, e.g., C II*, Si II, Fe II, Cr II, Al II and Al III, and the high-ionization species C IV and Si IV. The column densities were derived via Voigt-profile fitting of the absorption lines, using for each species the different transitions present in the spectrum. Fig. 3 and Fig. 4 show a sample of the fitted line profiles. For the strong C II* and Si II lines, nine components are needed to reproduce the profiles. Their redshifts (z_{abs}), column densities (log N in cm^{-2}) and turbulent broadening parameters (b_{turb} in km s^{-1}) are listed in Table 1. The components represent gas clouds associated with the DLA galaxy. The weaker lines were only detected in the two strongest components at $z_{abs} = 2.03937$ and 2.03954 (labeled components 6 and 7), which are responsible for the main absorption (log N(Si II)>15.2). It is important to note that 21 cm absorptions have been reported by Wolfe et al. (1985) in these two components. Most of the neutral hydrogen is therefore probably associated with these two components. The 21 cm ab-

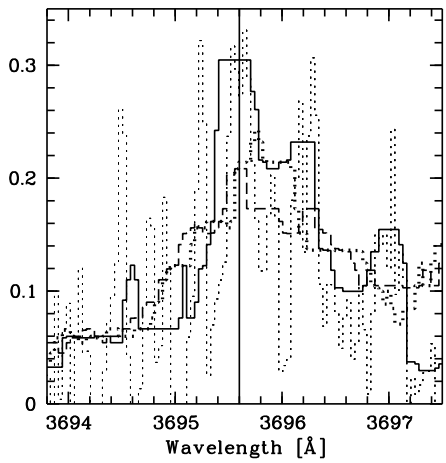

Fig. 2. Inset of the spectrum showing the Lyman-α emission line centered at 3695.6 Å. The thin dotted line is the initial high-resolution spectrum. The solid, thick dotted and dashed lines show the emission line smoothed with filter width of 5, 15 and 20 pixels respectively. Depending on the filter width the location of the peak of the emission varies by ∼ 0.2 Å.

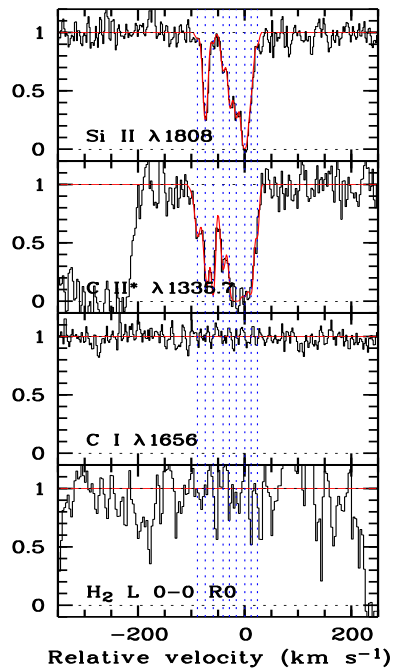

Fig. 3. Absorption line profiles of the C II*λ1335 doublet and the Si IIλ1808 transition. Nine individual components were needed to perform the fit to the absorption lines that is overplotted to the data as a solid line. The components are indicated by vertical dashed lines. The portions of the spectrum where the C Iλ1656 and H_2L0R0 transitions are expected are also shown. The zero point of the velocity scale has been taken at $z_{\rm abs}$ = 2.03954.

sorption is stronger at $z_{\rm abs}$ = 2.03937 than at $z_{\rm abs}$ = 2.03954 in accordance with the C II* absorption. Other species and in particular Si II show the contrary; their column densities are higher in component 7 than in component 6. Our column density determinations compare well with that of Prochaska & Wolfe (1999) except for Fe II that we find 0.2 dex less abundant based on the Fe IIλ1611 optically thin transition.

Assuming that these two components dominate the DLA system and contain most of the neutral hydrogen, we derived the total column densities from these two components and the corresponding abundances relative to solar ([X/H] = log (X/H) − log $(X/H)_\odot$). The solar values were taken from Morton (2003). The H I column density cannot be constrained for individual components. Therefore, taking into account only the column density summed over the two strongest components of the system can introduce a systematic error in the sense that our derived metallicities could be lower limits. We can estimate the possible corresponding error by integrating the column densities for all components of Si II (Table 1) and comparing with the value obtained for the two strongest components (Table 2). In this way we derive a metallicity for silicon of [Si/H] =−1.11 instead of −1.28, which means that the metallicity of silicon could be underestimated by at most 0.17 dex.

From the values in Table 2, we can derive abundance ratios for different metals. In the ISM of our Galaxy, zinc and silicon are barely depleted onto dust-grains which is consistent with our observed ratio in this high redshift system of [Si II/Zn II] = −0.06. Other elements appear depleted: chromium ([Cr II/Zn II] = −0.44), iron ([Fe II/Zn II] = −0.65), phosphorus ([P II/Zn II] = −0.32) and manganese ([Mn II/Zn II] = −0.83). The depletion of iron compared to zinc is indicative of the presence of dust at a level compatible with the presence of molecular hydrogen (see Ledoux et al. 2003). The fact that molecular hydrogen is *not* detected (log $N(H_2)$ < 14.9 and log f < −6.52) is therefore surprising, especially as the system has one of the highest H I column densities observed in DLAs (see Section 7).

Table 1. Redshifts, ion column densities and turbulent broadening parameters for all components of the system

#	$z_{\rm abs}$	log N(C II*)	log N(Si II)	$b_{\rm turb}$ [km s^{-1}]
1	2.03864	13.16±0.23	< 14.37[a]	5.4±4.1
2	2.03879	13.48±0.21	15.19±0.03	4.7±0.4
3	2.03894	14.43±0.31	< 14.37[a]	∼ 2.5
4	2.03913	13.55±0.15	14.65±0.10	5.2±1.8
5	2.03925	< 13.12[a]	14.99±0.10	4.3±1.4
6	2.03937	14.79±0.39	15.21±0.09	5.9±2.0
7	2.03954	13.91±0.65	15.90±0.20	5.3±0.9
8	2.03966	13.89±0.34	14.87±0.31	5.2±3.2
9	2.03978	< 13.12[a]	< 14.37[a]	2.5±4.4

[a] 5σ detection limit.

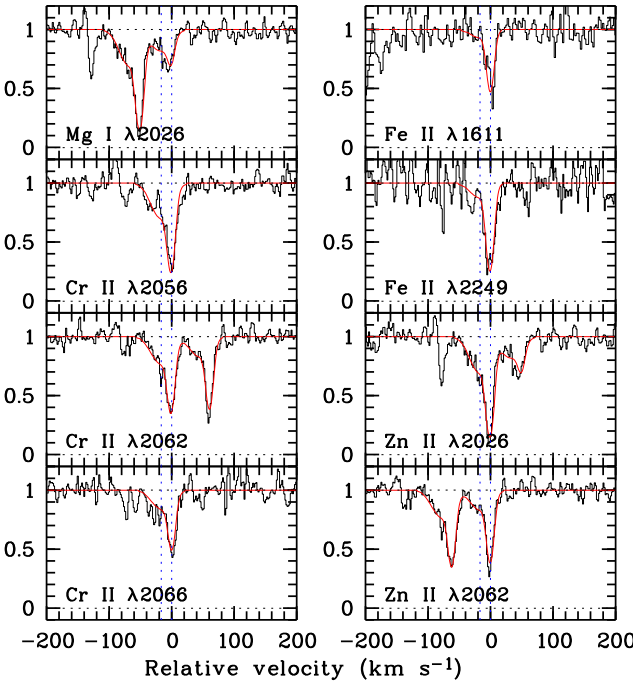

Fig. 4. Voigt-profile fits to the Fe II, Cr II, Zn II and Mg I absorption lines. When lines are blended simultaneous fits were performed. The zero point of the velocity scale has been taken at $z_{\rm abs} = 2.03954$.

Table 2. Ion column densities and metal abundances in components 6 and 7

Species	log N(X)	log(X/H)$_\odot$ + 12[a]	[X/H][b]
H I	21.70±0.10	...	...
H_2 (J=0)	<14.55	...	...
H_2 (J=1)	<14.60	...	...
C I	<12.45	...	...
C II*	14.84±0.35	...	...
Mg I	13.26±0.04	...	...
Mg II	16.07±0.07	7.58	−1.21±0.12
Si II	15.98±0.17	7.56	−1.28±0.20
P II	13.72±0.04	5.56	−1.54±0.11
Cr II	13.73±0.02	5.69	−1.66±0.10
Mn II	13.18±0.04	5.53	−2.05±0.11
Fe II	15.33±0.04	7.50	−1.87±0.11
Zn II	13.15±0.02	4.67	−1.22±0.10

[a] Reference abundances from Morton (2003).
[b] The given errors correspond to errors in the column densities.

5. Kinematics

Figure 5 shows the velocity profiles of several low (C II, C II*, Si II, Fe II, Al II, Al III) and high (C IV, Si IV) ionization metal absorption lines. The zero point of the velocity scale is located at $z_{\rm abs} = 2.03954$ and corresponds to the position of the strongest Fe II and Zn II component (see Fig. 4). We indicate in Fig. 5 the position of the peak of the Lyman-α emission line as a vertical solid line ($\Delta v \approx +45$ km s^{-1}). As can be seen from the figure the metal absorption lines are all blueshifted with respect to the Lyman-α emission. This is a consequence of kinematics either in the disk of a galaxy or in outflowing gas. We shall discuss both possibilities in more detail below.

5.1. Rotating disk

Prochaska & Wolfe (1997) made the case that the kinematics of DLA systems can be explained by models of large rotating disks. For the most likely rapidly rotating thick disk model they found that the absorption profile should be asymmetric with the strongest absorption component located at one edge of the profile. In this model the emission originating from the central part of the disk should be offset from the absorptions. This corresponds to what we observe in the DLA towards PKS 0458−020. Indeed, the velocity profiles of all metal absorption lines are observed blueward of the Lyman-α emission and the strongest absorption component is located at the red edge of the profile. In addition, the Lyman-α emission is located outside of the absorption profile at $\Delta v = 45 \pm 16$ km s^{-1} (the uncertainty comes from the uncertainty in the redshift of the Lyman-α emission) redward of the strongest absorption component. If we assume that the line of sight goes through a large rotating disk and the Lyman-α emission originates from the center of this disk, the blueshift of the low-ionization transition lines compared to the Lyman-α emission can be explained by gas that takes part in the rotation of the disk and is moving towards us. The small velocity offset of the strongest absorption compared to the emission suggests that the line of sight crosses the mid-plane of the disk far from the major axis, where the projected rotational velocity is small. The impact parameter between the line of sight and the center of the disk should be small and the inclination high to ensure strong enough absorption spread over more than 100 km s^{-1}. A small impact parameter between the emitting region and the line of sight was derived by Møller et al. (2004) of the order of 0.3 arcsec or 2.5 kpc. It is striking that the observed situation here corresponds to Case 4 of Figure 14 in Prochaska & Wolfe (1997) and supports the case for a large rotating disk. Note that the same conclusion has been drawn from 21 cm observations by Wolfe et al. (1985). This scenario assumes that the Lyman-α emission line peak records the systemic velocity of the galaxy. This may not be the case as indicated by the velocity shifts usually observed between the Lyman-α and the [O III] emissions in Lyman break galaxies (Pettini et al. 2001) or in DLA systems (Weatherley et al. 2005).

5.2. Galactic wind

On the other hand, the observed situation is also reminiscent of a wind flowing out of a star-forming region in our direction as observed in star-burst galaxies (e.g., Veilleux et al. 2005). The velocity offsets derived here for the strongest absorption components seem too small to be caused by a wind. We note that the high-ionization lines Si IV $\lambda\lambda$1393,1402 and C IV $\lambda\lambda$1548,1550 show a second broad absorption component at a projected velocity of −170 km s^{-1}. This strong feature is completely absent

in the lower ionization lines. There are two possibilities to explain this high-ionization region. Either the absorption comes from a region of hot gas associated with the DLA absorber but located at the projected distance corresponding to $v = -170$ km s^{-1}, or there is hot gas moving towards us with this velocity which has been ejected by the DLA galaxy. The first explanation is unlikely as in that case the gas should be located close to the center of the galaxy for the rotation velocity to be large and should therefore be associated with less ionized gas. The observed high velocity offset component could be a heated shock front or the galactic wind itself. However, this is clear indication for a galactic outflow driven by the mechanical energy deposited by supernova and stellar winds in star-forming regions. Blueshifted absorption and redshifted Lyman-α emission is also seen in high-redshift spectra of UV-selected galaxies and is also interpreted to be caused by winds (see Adelberger et al., 2005, and references therein). For a sample of Lyman-break galaxies, Pettini et al. (2001) showed that the Lyman-α emission is redshifted by 200 to 1100 km s^{-1} relative to the position of optical emission lines (Hβ and [O III]) and that the absorptions for three-quarters of the sample are blueshifted by a median value of -300 km s^{-1}. They interpret this as the signature of strong galactic winds. In this scenario, the gas seen in absorption in front of the stars is the approaching part of an expanding shell of swept-up material that has a very high optical depth to Lyman-α photons, so that the only detectable Lyman-α emission along the line of sight is from the back of the shell, behind the stars, receding at velocities where no foreground absorption takes place (Pettini et al. 2001). This is in agreement with the asymmetric Lyman-α emission line profile we observe, although the observed velocity range of $\Delta v = 120$ and 200 km s^{-1} for the low and high-ionization species respectively in the DLA towards PKS 0458−020 is smaller than the above findings. Weatherley et al. (2005) presented the detection of [O III] emission from galaxies responsible for two other damped Lyman-α systems. The velocity differences between the Lyman-α emission and the [O III] lines is about 100 km s^{-1} in both systems. Rest-frame optical emission lines are unaffected by resonant scattering and provide a better measurement of the galaxy systemic velocity. Therefore, the detection of [O III] emission lines from the galaxy in PKS 0458−020 could help to pin down the systemic velocity and to better determine the situation.

In this context, we note that the red wing of the C II* λ1335 absorption profile in Fig. 5 follows exactly the red wing of the C IV λ1548 profile (the profile of the C II λ1334 line is broader). This implies that at least part of the C II* absorption comes from the warm gas and is closely associated with the C IV phase. This supports the conjecture that part of the gas is outflowing.

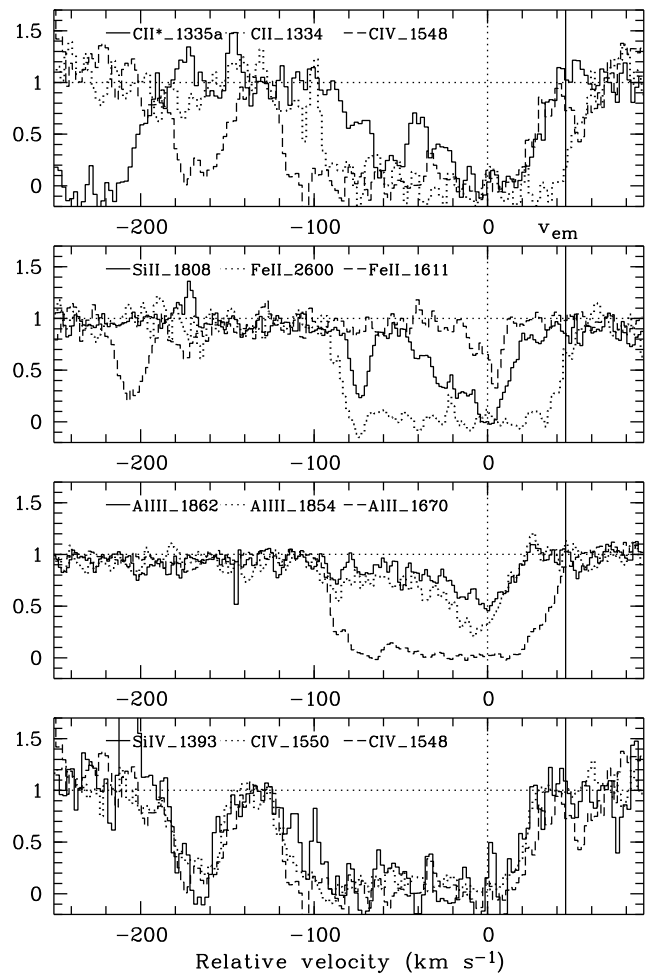

Fig. 5. Velocity profiles of different metal absorption lines. The dashed vertical line marks the zero point derived from the Fe IIλ1611 absorption (see second panel from top). The peak of the Lyman-α emission indicated by the vertical black solid line is offset by about 45 km s^{-1} redward of the main absorption component. The zero point of the velocity scale has been taken at $z_{\rm abs} = 2.03954$.

6. The star formation rate from C II*

In Section 3, we obtained the SFR in the DLA from the Lyman-α emission line flux. Wolfe et al. (2003) proposed another technique to derive the SFR in DLA systems from the strength of the C II* absorption and the dust-to-gas ratio under the assumption that the gas in DLAs is heated by the same mechanism responsible for the heating of the ISM in the Milky Way. The authors argue that under steady-state conditions the cooling rate measured from the C II* absorption equals the heating rate per H atom, which can be used to infer the SFR per unit area $\dot{\psi}^*$. While the C II* absorption strength is measured locally along the line of sight, the derived SFR per unit area is thought to represent the mean SFR over the whole star-forming volume in the DLA.

For PKS 0458−020, Wolfe et al. (2003) derived two solutions for the SFR per unit area of $\dot{\psi}^* \approx 10^{-2}$ or 10^{-1} M$_\odot$ yr^{-1} kpc^{-2} together with a gas particle density of $\log n \approx 1.2$ or 0.3 cm^{-3} assuming that the gas where the C II* absorption occurs is respectively cold or warm. Recent revision of the UV background spectrum indicates that these SFRs could be slightly overestimated (Wolfe 2005). Note that, by combining the above values of the particle density with our measured H I column density, we can derive a characteristic length scale for the light path through the H I absorbing region of ∼0.1 or 0.8 kpc. Obviously, the physical size of the

DLA galaxy is larger than this and therefore also the region over which the above mean star formation rates apply.

If the observed Lyman-α emitting region is the only source of heating, then we can derive the size of the heated region by equating the SFR from the Lyman-α emission to that derived from C II*. This size should be of the order of $R = 7.2$ or 2.3 kpc, respectively for the cold or warm gas, in order for the two SFR estimates to match. Note that this size is probably smaller than the total size of the H I disk, $R_{\rm disk}$. In the following, we try to estimate R. The first estimate can be obtained by assuming that the impact parameter between the Lyman-α emitting region and the line of sight corresponds to a lower limit of R. Møller et al. (2004) estimate this impact parameter to be $b_{\rm DLA} = 0\farcs3 \pm 0\farcs3$. Assuming the above cosmology (see Sect. 3), a redshift of $z = 2.04$ corresponds to an angular diameter distance to the DLA of 1723 Mpc, so that the angle of $0\farcs3$ corresponds to a proper size of 2.5 kpc. This value coincides with the above solution if the gas is warm. For the cold gas solution, this rather small value can be explained by the fact that the measured impact parameter can lie anywhere in the range $[0; R_{\rm disk}]$.[1].

Another estimate of R can be derived by using high-resolution radio interferometry observations in front of the extended PKS 0458−020 radio source. Briggs et al. (1989) probed several different paths through the absorbing medium and concluded that the absorber is a disk-like structure that extends across 2″. This corresponds to a radius of $R_{\rm disk} = 8.4$ kpc. The disk should be oriented in the same direction as the radio source and therefore in the South-Western direction whereas the Lyman-α emitting region is in the North-Western direction. This is consistent, as are the kinematics, with the existence of an inclined large disk with its center at the location of the emitting region. Therefore a large value of R is not incompatible with this model.

On this basis alone, it is therefore difficult to decide whether the gas is cold or warm. Another way of looking at this problem is to estimate the mean UV flux along the line of sight.

7. Missing molecules

Molecular hydrogen is not detected in our spectrum down to a limit of $\log N(H_2) = 14.9$, corresponding to a molecular fraction ($f = 2N(H_2)/[2N(H_2) + N(H\,I)]$) of $\log f = -6.52$. The absence of molecules is surprising at such a high H I column density ($\log N(H\,I) = 21.7$). As the gas is probably dusty with a depletion factor of [Zn/Fe] = 0.65, this could be a consequence of high temperature and/or high UV background radiation.

The temperature of the gas can be estimated from the spin temperature. Absorption at 21 cm was reported in two components at the same redshifts as our components 6 and 7 (Wolfe et al. 1985; see Table 1). Combining the 21 cm absorption with the H I column density, Wolfe et al. (1985) estimated the spin temperature of the gas to be less than 1000 K. Kanekar & Chengalur (2003) corrected this value to $T_{\rm S} \sim 385 \pm 100$ K. This is unusually low for a DLA system and is in the range of Galactic values (<350 K; Braun & Walterbos 1992).

The integrated 21 cm optical depth of component 6 is about four times larger than that of component 7 in accordance with what is seen for the C II* absorption. It is however apparent that the metal column densities are smaller in component 6 (see Fig. 4); the Si II column density is for example five times smaller in component 6 than in component 7. On the basis of this inverted ratio, if we assume similar physical conditions (metallicity and ionization factor) in both components, then the H I column density is smaller in component 6 than in component 7 by a factor of five and the spin temperature is smaller by a factor of twenty. Conversely, assuming a similar temperature would lead to a metallicity ten times smaller in component 6 which would be at odds with the high homogeneity of the gas usually seen in DLA systems (see Rodriguez et al. 2005). The above temperature of 385 K is the harmonic mean between the temperatures in the two components weighted by the H I column densities. Given the above ratio, we conclude that the spin temperatures of components 6 and 7 are of the order of 2000 and 100 K respectively.

Using the SFR from the Lyman-α emission and the relation between SFR and UV flux, SFR $= L_{\rm UV} \times 1.4 \times 10^{-28}$ (Kennicutt et al. 1998), we derive a specific UV luminosity of $L_{\rm UV} = 1.14 \times 10^{28}$ erg s^{-1} Hz^{-1} in the frequency range between 1500 and 2800 Å. This luminosity corresponds to a UV flux of $F_{\rm UV} = 1.53 \times 10^{-17}$ erg s^{-1} cm^{-2} Hz^{-1} if we assume that the distance to the absorbing gas is given by the impact parameter. The resulting flux is ten times larger than the UV flux measured in the ISM of our Galaxy ($F_{\rm UVgal} = 1.47 \times 10^{-18}$ erg s^{-1} cm^{-2} Hz^{-1} following the fit in Appendix 1 of Péquignot & Aldrovandi 1986). Therefore, the absence of molecular hydrogen is not surprising even though at least part of the gas is at low temperature and the depletion factor is not small ([Zn/Fe] = 0.65), indicating that dust is present in the gas. As shown by the models of Srianand et al. (2005), the absence of H_2 can be explained as the consequence of the high radiation field.

Note that this is consistent with the high mean ambient UV flux derived by Wolfe et al. (2004; >19.1 times the Galactic value).

8. Summary and conclusions

We have presented the high-resolution spectrum of the strong damped Lyman-α absorber at $z_{\rm abs} = 2.03954$ in front of PKS 0458−020. It is one of the rare systems where Lyman-α is clearly seen in emission with an impact parameter between the emitting region and the line of sight of ∼0.3 arcsec (Møller et al. 2004) or 2.5 kpc for the adopted concordance cosmology. We determined the redshift of the Lyman-α emission line to be $z = 2.0400 \pm 0.0002$. The metal absorption lines are found to be blueshifted compared to the Lyman-α emission and to span a velocity range of $\Delta v = 120$ and 200 km s^{-1} for the low and high-ionization species respectively. The kinematics, together with the observations in 21 cm by Briggs et al. (1989), are strikingly consistent with the model of a large rotating disk presented by Prochaska & Wolfe (1997) in which the line of sight

[1] Møller et al. (2004) also give a firm upper limit for the impact parameter of $b_{\rm DLA} = 0\farcs8$, by which the object would fall outside the slit in their observations. This value corresponds to a proper size of 6.7 kpc

crosses the mid-plane far from the center of the disk but keeps a low impact parameter with the center of the disk. Conversely, the coincidence of the red wings of the C IV and C II* profiles and the extent of the C IV absorption argues for the presence of blueshifted warm gas possibly part of an outflow from the DLA galaxy. If true, the velocity of such outflows is much smaller than what is observed in star-burst galaxies (see Veilleux et al. 2005). A possible detection of rest-frame optical emission lines could help to support the model of a large rotating disk.

We derived column densities and metallicities for a number of species. The DLA absorber corresponds to a two-phase medium with warm and cold gas. We could compare the star formation rate derived from the Lyman-α emission line with the derivation from the C II* method in the same object. From the Lyman-α emission, we find a star formation rate of SFR = $1.6^{+0.6}_{-0.3}$ $M_\odot$ yr^{-1}. From the C II* column density, Wolfe et al. (2003) derived a SFR per unit area of 10^{-2} and 10^{-1} $M_\odot$ yr^{-1} kpc^{-2} for respectively cold and warm gas. This means that the diffuse gas should be extended over a radius of ∼7.2 or 2.3 kpc respectively for both SFRs to match.

The absence of molecular hydrogen to a limit of $\log f = -6.52$ can be explained as the consequence of the high radiation field in the disk due to star formation. The ambient UV flux due to the observed emitting region is one order of magnitude larger than the flux in our Galaxy.

Acknowledgements. JH and SC acknowledge the support of the European Community under a Marie Curie Host Fellowship for Early Stage Researchers Training under contract number MEST-CT-2004-504604. RS and PPJ gratefully acknowledge the Indo-French Centre for the Promotion of Advanced Research (Centre Franco-Indien pour la Promotion de la Recherche Avancée) under contract No. 3004-3. PPJ thanks IUCAA for hospitality during the time part of this work has been completed. We thank the referee, Steve Warren, for a careful reading of the manuscript and for providing comments that helped to improve the paper.

References

Adelberger, K. L., Shapley, A. E., Steidel, C. C., Pettini, M., Erb, D. K., & Reddy, N. A. 2005, ApJ, 629, 636
Ballester, P., Dorigo, D., Disarò, A., Pizarro de La Iglesia, J. A., Modigliani, A., & Boitquin, O. 2000, ASPC, 216, 461
Braun, R., Walterbos, R. A. M. 1992, ApJ, 386, 120
Briggs, F. H., Wolfe, A. M., Liszt, H. S., et al. 1989, ApJ, 341, 650
Chen, H.-W.,& Lanzetta, K. M. 2003, ApJ, 597, 706
Curran, S. J., Webb, J. K., Murphy, M. T., Bandiera, R., Corbelli, E., & Flambaum, V. V. 2002, PASA, 19, 455
Dekker, H., D'Odorico, S., Kaufer, A., Delabre, B., & Kotzlowski, H. 2000, SPIE, 4008, 534
Kanekar, N., & Chengalur, J.N. 2003, A&A, 399, 857
Kennicutt, R.C. 1998, ARA&A, 36, 189
Le Brun, V., Bergeron, J., Boissé, P., Deharveng, J. M. 1997, A&A, 321, 733
Ledoux, C., Bergeron, J., & Petitjean, P. 2002, A&A, 385, 802
Ledoux, C., Petitjean, P., & Srianand, R. 2003, MNRAS, 346, 209
Møller, P., Fynbo, J.P.U.,& Fall, S.M. 2004, A&A, 422, L33
Møller, P., Warren, S. J., Fynbo, J. P 1998, A&A, 330, 19
Møller, P., & Warren, S. J. 1993, A&A, 270, 43
Morton, D. C. 2003 ApJS, 149, 205
Péquignot, D., & Aldrovandi, S. M. V. 1986, A&A, 161, 169
Petitjean, P., Srianand, R.,& Ledoux, C. 2000 A&A, 364, L26
Pettini, M., Shapley, A. E., Steidel, C. C., Cuby, J.G., et al. 2001 ApJ, 554, 981
Pettini, M., Smith, L. J., Hunstead, R. W., & King, D. L. 1994 ApJ, 426, 79
Prochaska, J.X.,& Wolfe, A.M. 1997 ApJ, 487, 73
Prochaska, J.X.,& Wolfe, A.M. 1999 ApJS, 121, 369
Rodriguez, E., Petitjean, P., Aracil, B., Ledoux, C., & Srianand, R. 2005, A&A, accepted
Srianand, R., Shaw, G., Ferland, G., Petitjean, P., & Ledoux, C. 2005, astro-ph/0506556
Veilleux, S., Cecil, G., & Bland-Hawthorn, J. 2005 astro-ph/0504435
Vreeswijk, P.M. et al. 2004, A&A, 419, 927
Warren, S. J., Møller, P., Fall, S. M., & Jakobsen, P. 2001 MNRAS, 326, 759
Weatherley, S. J., Warren, S. J., Mller, P., Fall, S. M., Fynbo, J. U.,& Croom, S. M. 2005, MNRAS, 358, 985
Wolfe, A. M., 2005, in "Probing Galaxies Through Quasar Absorption Lines". IAU Symposium 199, eds P. R. Williams, C, Shu, B. Ménard, Shanghai
Wolfe, A. M., Briggs, F. H., Turnshek, D. A., Davis, M. M., Smith, H. E., & Cohen, R. D. 1985, ApJ, 294, L67
Wolfe, A.M., Howk, J. C., Gawiser, E., Prochaska, J.X.,& Lopez, S. 2004, ApJ 614, 625
Wolfe, A. M., Prochaska, J. X., & Gawiser, E. 2003, ApJ, 593, 215